MITSUBISHI ELECTRIC RESEARCH LABORATORIES
https://www.merl.com

A Novel High-Frequency Injection Method Towards Speed-Sensorless Drive Control of Induction Machines over Full Speed Range

Wu, Jingjie; Goldsmith, Abraham; Zhou, Lei; Liu, Dehong; Wang, Bingnan; Wang, Yebin

TR2025-061 May 20, 2025

Abstract

This paper proposes a systematic experimental procedure to exploit the torque capability of sensorless induction machine (IM) control at/near zero frequency/speed under high- frequency signal injection (HFSI). The key idea is to select the tilted injection angle by two criteria: (1) maintaining the polarity of the sensitivity of an error signal w.r.t. the rotor flux angle estimation error to ensure closed-loop stability, and (2) maximizing the sensitivity to ensure robustness against uncertainties. Three look-up tables (LUTs) of injection angles and error scalings are constructed regarding operating points and used for real-time HFSI implementation. We further integrate the proposed HFSI method with an adaptive flux observer (AFO) to enable a stable sensorless torque control at full-speed range. Experiment results validate the sensorless IM's torque capability and demonstrate a smooth operation over the full speed range of the proposed unified observer.

IEEE International Electric Machines and Drives Conference (IEMDC) 2025

Mitsubishi Electric Research Laboratories, Inc.
201 Broadway, Cambridge, Massachusetts 02139

A Novel High-Frequency Injection Method Towards Speed-Sensorless Drive Control of Induction Machines over Full Speed Range

Jingjie Wu
Wisconsin Electric Machines and Power Electronics Consortium
University of Wisconsin-Madison
Madison, USA
jingjie.wu@wisc.edu

Abraham Goldsmith
Mitsubishi Electric Research Laboratories (MERL)
Cambridge, MA 02139 USA
goldsmith@merl.com

Lei Zhou
Wisconsin Electric Machines and Power Electronics Consortium
University of Wisconsin-Madison
Madison, USA
lei.zhou@wisc.edu

Dehong Liu
Mitsubishi Electric Research Laboratories (MERL)
Cambridge, MA 02139 USA
liudh@merl.com

Bingnan Wang
Mitsubishi Electric Research Laboratories (MERL)
Cambridge, MA 02139 USA
bwang@merl.com

Yebin Wang
Mitsubishi Electric Research Laboratories (MERL)
Cambridge, MA 02139 USA
yebinwang@merl.com

***Abstract*—This paper proposes a systematic experimental procedure to exploit the torque capability of sensorless induction machine (IM) control at/near zero frequency/speed under high-frequency signal injection (HFSI). The key idea is to select the tilted injection angle by two criteria: (1) maintaining the polarity of the sensitivity of an error signal w.r.t. the rotor flux angle estimation error to ensure closed-loop stability, and (2) maximizing the sensitivity to ensure robustness against uncertainties. Three look-up tables (LUTs) of injection angles and error scalings are constructed regarding operating points and used for real-time HFSI implementation. We further integrate the proposed HFSI method with an adaptive flux observer (AFO) to enable a stable sensorless torque control at full-speed range. Experiment results validate the sensorless IM's torque capability and demonstrate a smooth operation over the full speed range of the proposed unified observer.**

***Index Terms*—Induction machine drive, sensorless control, high-frequency signal injection, unified observer.**

I. Introduction

In high-performance induction motor (IM) drives, shaft sensors are commonly used to measure the rotor speed and estimate the rotor flux angle for implementing indirect field-oriented control (IFOC) [1]. However, the sensors increase the cost and size of the system, reduce the overall reliability and may not be suitable to install in harsh environment. To address these challenges, significant research efforts in recent years have focused on developing speed sensorless control techniques for IM drives. Most existing sensorless control methods can roughly be classified into two main categories: the signal-injection-based approach and the model-based approach.

Among the signal-injection-based approaches, High-frequency signal injection (HFSI) methods have been widely utilized for sensorless IM control, where the injection frequency much higher than the fundamental frequency. These methods heavily rely on the machines' magnetic saliency and can be classified into two main categories: rotating signal injection in stationary reference frame and pulsating signal injection in estimated synchronous reference frame [2]. The rotating signal injection scans through all anisotropies existing in the machine including saturation, rotor slotting and engineered saliencies [3]. On the other hand, the pulsating signal injection can be applied to an direction with educated guess and thus maximize the sensitivity of locating a target saliency [4]. Tracking saturation-induced saliency can provide rotor flux angle information at zero or low frequency operation, which is suitable for torque control and less accurate speed regulation [5]. Square-wave HF pulsating voltage injection are widely adopted due to its high estimation bandwidth compared to traditional sinusoidal-wave injection and has demonstrated excellent estimation performance [6]. However, such sensorless operation becomes challenging in heavy-load condition as the significant cross-saturation shifts the convergence points and degrades the sign-to-noise ratio (SNR) and stability [7]. Many methods have been proposed to enhance the operation limit and the robustness for interior permanent magnet synchrnous machine (IPMSM) HFSI sensorless control [8]. However, there are only few existing analytical and experimental research effort on HFSI for IM on this topic.

In addition, HFSI method is typically effective only in zero-to-low speed range, and its performance significantly deteriorates in medium-to-high speed range where the model-based approach can achieve excellent estimation and performance. To achieve full-speed-range sensorless control, as required in many applications, it is natural to consider combining the HFSI and model-based approaches as complement for each other. However, there are only few research effort on this aspect for IM. In [**?**], low-frequency signal injection (LFSI) is used to enhance a adaptive flux observer (AFO) by combining the error signals with a weighted sum. [9] proposes a hybrid speed estimator by combining the estimated speed from a model-based observer and HFSI observer. Despite the effectiveness, the stability of these approaches is not guaranteed, the estimation dynamics can be nonsmooth, and the tuning of weighting parameters requires significant effort.

In order to overcome the aforementioned challenges, this paper proposes a systematic experimental procedure, called perturbed convergence analysis, to fully exploit the sensorless HFSI torque capability from adopting tilted HF voltage signal injection with additional error compensation. The tilted angle, error offset and error scaling are constructed as three look-up-tables (LUT) in terms of the loading conditions to achieve excellent dynamic performance in real time. Besides, this paper further proposes a novel unified observer combining the proposed HFSI estimator with AFO to achieve smooth sensorless operation at full-speed range. Experimental evaluations on a IM testbed validate the perturbed convergence analysis procedure and is able to extend the HFSI torque capability up to rated torque. Two tests on the unified observer demonstrate a smooth closed-loop dynamic performance and a stable speed estimation over full speed range.

II. Problem Statement

Fig. 1 illustrates the reference frame and the relative angle definition where $\alpha\beta s, dqr, dq\hat{r}, dqh$ represent the stationary, rotor flux, estimated rotor flux and voltage injection reference frames, respectively. The superscript "r", "$\hat{r}$" and "h" mean that the variable is expressed in rotor flux, estimated rotor flux and voltage injection reference frames, respectively. The superscript "$*$" indicates a reference command. The subscript "r", "s" and "h" represents the rotor, stator and HF component, respectively.

A. High-Frequency Injection Sensorless Control for IM

High-frequency signal injection (HFSI) method is adopted here to achieve stable sensorless control at zero-to-low frequency range by exploiting the spatial saliency of the IM. In this paper, we only focus on the saturation-induced saliencies from the main magnitizing flux or localized leakage flux [5]. Considering such inductance saturation, the HF voltage model for IM in rotor flux-oriented reference frame, assuming that the resistive voltage drop and back-EMF are negligible, can be expressed as

$$\begin{bmatrix} v^r_{dsh} \\ v^r_{qsh} \end{bmatrix} = \begin{bmatrix} L_{dh} & L_{dqh} \\ L_{dqh} & L_{qh} \end{bmatrix} \frac{d}{dt} \begin{bmatrix} i^r_{dsh} \\ i^r_{qsh} \end{bmatrix}, \tag{1}$$

where v_{dsh}, v_{qsh} are the HF stator voltage in d- and q-axes; i_{dsh}, i_{qsh} are the HF stator current in d- and q-axes; L_{dh} and L_{qh} are the incremental transient self inductance in d- and q-axes; L_{dqh} is the incremental transient mutual inductance due to cross-saturation.

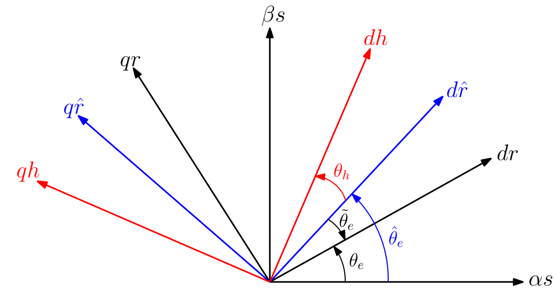

Fig. 1: Definitions of angles and axes.

Here, we adopt a pulsating square-wave voltage injection with frequency being half of the PWM switching frequency to improve the sensorless estimation bandwidth and closed-loop dynamic performance [10]. For conventional HFSI sensorless control of IM, the HF square-wave voltage signal is injected into the $d\hat{r}$ axis in voltage injection reference frame as

$$\begin{bmatrix} v^{\hat{r}}_{dsh} \\ v^{\hat{r}}_{qsh} \end{bmatrix} = \begin{bmatrix} v_h[n] \\ 0 \end{bmatrix} = \begin{bmatrix} V_h \\ 0 \end{bmatrix} \cdot (-1)^n, \quad n = 0, 1, 2, \cdots \tag{2}$$

where V_h is the voltage injection magnitude, n is the number of sampling period. By transforming between dr and $d\hat{r}$ reference frames for (1), the HF current variation induced by (2) at $q\hat{r}$-axis between adjacent sampling points can be obtained as [10]

$$\Delta i^{\hat{r}}_{qsh} = \frac{V_h \Delta T}{L_n} \sin(-2\tilde{\theta}_e + \theta_m) \cdot (-1)^{n-1}, \quad n = 1, 2, \cdots, \tag{3}$$

where ΔT is sampling period, θ_m stands for the cross-saturation angle due to L_{dqh} and all parameters are defined as

$$\theta_m = \tan^{-1}(\frac{-L_{dqh}}{L_{sd}}), \ L_n = \frac{L_{dh}L_{qh} - L^2_{dqh}}{\sqrt{L^2_{sd} + L^2_{dqh}}}, \tag{4}$$

where $L_{sd} = (L_{qh} - L_{dh})/2$. The error signal for rotor flux estimation can be obtained as

$$\epsilon = \frac{1}{i_\Delta} \cdot \Delta i^h_{qsh} \cdot (-1)^n = \frac{L_{n0}}{L_n} \sin(2\tilde{\theta}_e - \theta_m), \tag{5}$$

where $i_\Delta = \frac{V_h \Delta T}{L_{n0}}$ and L_{n0} is computed from (4) using nominal L_d, L_q value with no cross-saturation. The error signal (5) is then sent to a phase-locked loop to estimate the rotor flux angle. If cross-saturation exists, i.e. $\theta_m \neq 0$, a position estimation error of $\tilde{\theta}_e = \frac{1}{2}\theta_m$ will occur, which requires a compensation on either the error or the estimated position. Although this approach is effective, the feasibility under different conditions remains to be investigated. A straightforward way is to evaluate the sensitivity of ϵ with respect to $\tilde{\theta}_e$ given $\tilde{\theta}_e \approx \frac{1}{2}\theta_m$ as

$$k_e = \frac{\partial \epsilon}{\partial \tilde{\theta}_e} \approx \frac{2L_{n0}}{L_n}, \tag{6}$$

where k_e indicates the observation capability of the position estimation error. If there is no saturation in ideal condition, i.e., $L_{dh} = L_{qh}$ and $L_{dqh} = 0$, the sensitivity k_e is always zero, which means HFSI is infeasible. For IM with saturation, the sensitivity k_e varies according to the operating points (i^*_{ds}, i^*_{qs}) which affects L_n. In general, a larger i^*_{qs} for a constant i^*_{ds} lowers the magnitude of k_e, which sets the torque limit for HFSI sensorless control. In conventional HFSI, the sensitivity k_e in (6) is fixed for each operating point, thereby limiting the potential to extend the torque capability. Therefore, the first problem this paper attempts to address can be formulated as follows.

Problem 1: Given the HF model (1), exploit the torque capability for HFSI sensorless control of IM by introducing extra degree of freedoms in signal injection and develop a systematic procedure with thorough theoretical analysis.

B. Baseline Adaptive Flux Observer

The HFSI can perform an accurate estimation of rotor flux position in zero-to-low speed range but degrades at medium-to-high speed range where the BEMF component becomes considerable. In this case, model-based observer stands for a good alternative for medium-to-high speed sensorless estimation and control.

In the rotor flux-oriented dqr reference frame where the d-axis is aligned with the rotor flux and rotating with speed ω_s, the mathematical model of an IM can be expressed as

$$\begin{aligned}\dot{\boldsymbol{x}}^r &= \mathbf{A}(\omega_s)\boldsymbol{x}^r + \mathbf{B}\boldsymbol{v}^r_{dqs},\\ \boldsymbol{y}^r &= \mathbf{C}\boldsymbol{x}^r,\end{aligned} \tag{7}$$

where

$$\boldsymbol{x}^r = \begin{bmatrix}\lambda^r_{ds}\\ \lambda^r_{qs}\\ \lambda^r_{dr}\end{bmatrix}, \quad \mathbf{A}(\omega_s) = \begin{bmatrix}\frac{-R_s}{L_s\sigma} & \omega_s & \frac{L_mR_s}{L_rL_s\sigma}\\ -\omega_s & \frac{-R_s}{L_s\sigma} & 0\\ \frac{L_mR_r}{L_rL_s\sigma} & 0 & -\frac{R_r}{L_r\sigma}\end{bmatrix},$$

$$\mathbf{B} = \begin{bmatrix}1 & 0\\ 0 & 1\\ 0 & 0\end{bmatrix}, \quad \boldsymbol{v}^r_{dqs} = \begin{bmatrix}v^r_{ds}\\ v^r_{qs}\end{bmatrix}, \quad \boldsymbol{y}^r = \begin{bmatrix}i^r_{ds}\\ i^r_{qs}\end{bmatrix},$$

$$\mathbf{C} = \begin{bmatrix}\frac{1}{L_s\sigma} & 0 & -\frac{L_m}{L_rL_s\sigma}\\ 0 & \frac{1}{L_s\sigma} & 0\end{bmatrix}.$$

Here $\lambda^r_{ds}, \lambda^r_{qs}$ are the stator fluxes in d- and q-axes; λ^r_{dr} is the rotor flux; R_s, R_r are the stator and rotor resistance; L_s, L_m, L_r are the stator, magnitizing and rotor inductance, respectively; $\sigma = 1 - \frac{L_m^2}{L_sL_r}$ is the leakage factor; v^r_{ds}, v^r_{qs} are the input voltage in d- and q-axes; i^r_{ds}, i^r_{qs} are the stator current in d- and q-axes.

The adaptive full-order flux observer in estimated $dq\hat{r}$ frame based on (7) can be constructed as follows

$$\begin{aligned}\dot{\hat{\boldsymbol{x}}} &= \mathbf{A}(\hat{\omega}_s)\hat{\boldsymbol{x}} + \mathbf{B}\boldsymbol{v}_{dqs} + \mathbf{L}(\boldsymbol{y} - \hat{\boldsymbol{y}}),\\ \hat{\boldsymbol{y}} &= \mathbf{C}\hat{\boldsymbol{x}},\end{aligned} \tag{8}$$

where $\hat{\boldsymbol{x}} = \begin{bmatrix}\hat{\lambda}^{\hat{r}}_{ds} & \hat{\lambda}^{\hat{r}}_{qs} & \hat{\lambda}^{\hat{r}}_{dr}\end{bmatrix}^\top$ is the estimated stator and rotor fluxes; $\hat{\boldsymbol{y}} = \begin{bmatrix}\hat{i}^{\hat{r}}_{ds} & \hat{i}^{\hat{r}}_{qs}\end{bmatrix}^\top$ is the estimated currents; $\boldsymbol{y} = \begin{bmatrix}i^{\hat{r}}_{ds} & i^{\hat{r}}_{qs}\end{bmatrix}^\top$ is the current measurement in estimated $dq\hat{r}$-axes; $\mathbf{L} \in \mathbb{R}^{3\times3}$ is the observer gain matrix. The error signal for estimating rotor speed is $e_{iqs} = i_{\widehat{qs}} - \hat{i}_{qs}$. Then, the estimated rotor speed, slip frequency, and synchronous speed can be estimated via a PI controller as follows

$$\dot{\hat{\omega}}_r = K_p(1 + \frac{K_i}{s})e_{iqs}, \tag{9}$$

$$\hat{\omega}_{sl} = \frac{L_mR_r}{L_rL_s\sigma}\frac{\hat{\lambda}_{\widehat{qs}}}{\hat{\lambda}_{\widehat{dr}}} + L_{42}e_{iqs}, \tag{10}$$

$$\hat{\omega}_s = \hat{\omega}_r + \hat{\omega}_{sl} \tag{11}$$

where L_{42} is an additional observer gain for slip frequency estimation. The rotor flux angle can be computed as

$$\hat{\theta} = \int \hat{\omega}_s \mathrm{d}t. \tag{12}$$

The flux and speed observer (8), (9) can achieve accurate speed estimation and stable sensorless operation at medium-to-high speed range. The second problem under investigation in this paper can be formulated as follows.

Problem 2: Develop a unified approach to combine the methods of HFSI in Sec. II-A and the baseline AFO observer to achieve smooth and stable sensorless control over full speed range.

III. HFSI Perturbed Convergence Analysis and Unified Observer

A. HFSI Perturbed Convergence Analysis

To extend the torque capability of HFSI, we introduce new degree of freedom by tilting the HF voltage injection axis onto the dh-axis in Fig. 1, which can be expressed as

$$\begin{bmatrix}v^h_{dsh}\\ v^h_{qsh}\end{bmatrix} = \begin{bmatrix}V_h\\ 0\end{bmatrix}\cdot(-1)^n, \quad n = 0, 1, 2, \cdots \tag{13}$$

where v^h_{dsh}, v^h_{qsh} are the HF stator voltage in injection reference frame. Similar to the computation in Section II-A, we can compute the HF current variation at qh-axis between adjacent sampling points as

$$\Delta i^h_{qsh} = \frac{V_h\Delta T}{L_n}\sin\left(2(\theta_h - \tilde{\theta}_e) + \theta_m\right)\cdot(-1)^{n-1}. \tag{14}$$

The estimation error signal can be extracted from (14) as

$$\epsilon = \frac{1}{i_\Delta}\cdot\Delta i^h_{qsh}\cdot(-1)^n = -\frac{L_{n0}}{L_n}\sin(2(\theta_h - \tilde{\theta}_e) + \theta_m). \tag{15}$$

To fully evaluate the sensitivity for feasibility, we perform a first-order Taylor expansion on (15) around $\tilde{\theta}_e = 0$ for an arbitrary operating point $\boldsymbol{i}^*_s = (i^*_{ds}, i^*_{qs})$ as

$$\epsilon = k_e(i^*_{ds}, i^*_{qs}, \theta_h)\tilde{\theta}_e + \epsilon_{comp}(i^*_{ds}, i^*_{qs}, \theta_h), \tag{16}$$

where

$$k_e = -L_{n0}\partial\frac{\sin(2(\theta_h - \tilde{\theta}_e) + \theta_m(i^*_{ds}, i^*_{qs}, \tilde{\theta}_e))}{L_n(i^*_{ds}, i^*_{qs}, \tilde{\theta}_e)}\Big/\partial\tilde{\theta}_e, \tag{17}$$

$$\epsilon_{comp} = -\frac{L_{n0}}{L_n(i^*_{ds}, i^*_{qs}, \tilde{\theta}_e = 0)}\sin(2\theta_h + \theta_m), \tag{18}$$

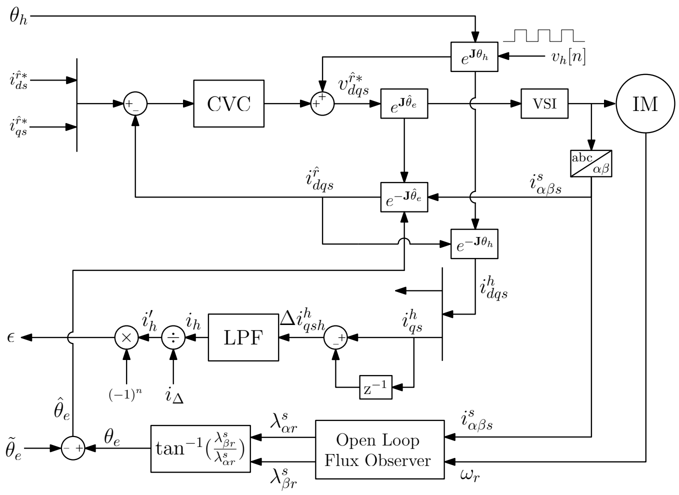

Fig. 2: Block diagram for Convergence Analysis.

where L_n, θ_m both depend on $\tilde{\theta}_e$ in practice since $\tilde{\theta}_e$ leads to the change of saturation level and inductance values. $k_e(\cdot)$ and $\epsilon_{comp}(\cdot)$ are the sensitivity and offset around $\tilde{\theta}_e = 0$. An operating point $\boldsymbol{i}_s^*$ is stabilizable for HFSI control if the sensitivity is positive, i.e., $k_e(\cdot) > 0$. A larger magnitude of $|k_e|$ indicates a higher signal-to-noise ratio (SNR) and better robustness against uncertainties and disturbances. By employing tilted injection, the sensitivity k_e and offset ϵ_{comp} in (17) become dependent on the tilted injection angle θ_h, which allows us to increase the magnitude of $|k_e|$ by varying θ_h and thus enhance the achievable torque range. Due to the shift-of-saliency (SOS), $\epsilon_{comp} \neq 0$ in general and conventional methods typically select θ_h such that $\epsilon_{comp} = 0$, which, however, ignores the aforementioned stabilizability criteria and thus renders unstable control at high torque command.

Distinctively, we propose a systematic experimental procedure, called perturbed convergence analysis, where we explicitly takes the stabilizability criteria into account. For each $\boldsymbol{i}_s^*$ operating point, the main objectives of the perturbed convergence analysis for HFSI sensorless control is to

1) choose the tilted injection angle $\theta_h(\boldsymbol{i}_s^*)$ to ensure $k_e(\cdot) > 0$ and then maximize the magnitude of $|k_e|$,
2) obtain the value of offset $\epsilon_{comp}(\boldsymbol{i}_s^*)$ for the selected θ_h with maximum $|k_e|$ such that this operating point can be a stable equilibrium,
3) record and use the maximum k_e value and offset ϵ_{comp} for computing the error signal from (15) as

$$\epsilon_{HFSI} = \tilde{\theta}_e = \frac{1}{k_e}(\epsilon - \epsilon_{comp}), \tag{19}$$

which is equivalent to fixing the PLL pole locations and enables a consistent dynamic performance over all operating conditions.

These tasks must be carried out for all desired operating points. A constant flux operation is considered in this paper where i_{ds}^* is chosen to be a constant. With all recorded values, three LUTs can be constructed as

$$\theta_h = f_1(\boldsymbol{i}_{qs}^*), \quad \epsilon_{comp} = f_2(\boldsymbol{i}_{qs}^*), \quad k_e = f_3(\boldsymbol{i}_{qs}^*), \tag{20}$$

for real-time signal injection and error computation based on $\boldsymbol{i}_{qs}^*$. To obtain the required data, the block diagram of the perturbed convergence analysis is shown in Fig. 2 where a speed sensor is required. The key idea is to intentionally introduce small perturbation in $\tilde{\theta}_e$ around 0 and then record the response of error signal ϵ to experimentally determine k_e and ϵ_{comp} from (16) for different θ_h. To control $\tilde{\theta}$, we propose to use an open-loop flux observer to estimated the flux angle using measured rotor speed as

$$\begin{aligned}
\dot{\lambda}_{\alpha r}^s &= -\frac{1}{\tau_r}\lambda_{\alpha r}^s + \frac{L_m}{\tau_r} i_{\alpha s}^s - \omega_r \lambda_{\beta r}^s, \\
\dot{\lambda}_{\beta r}^s &= -\frac{1}{\tau_r}\lambda_{\beta r}^s + \frac{L_m}{\tau_r} i_{\beta s}^s + \omega_r \lambda_{\alpha r}^s, \\
\theta_e &= \tan^{-1}\left(\frac{\lambda_{\beta r}^s}{\lambda_{\alpha r}^s}\right),
\end{aligned} \tag{21}$$

where $\lambda_{\alpha r}^s$ and $\lambda_{\beta r}^s$ are the rotor flux in stationary frame and ω_r is the electrical rotor speed obtained from sensor measurement. Using the flux angle computed from (21) as ground truth, we can control the $\tilde{\theta}$ by using $\hat{\theta}_e = \theta_e - \tilde{\theta}_e$ in the Park transform for current control. The detailed convergence analysis procedure according to Fig. 2 is illustrated in Algorithm 1. First, we grid the torque current i_{qs}^* and injection angle θ_h within respective ranges of interest as inputs. Second, implement i_{ds}^* and j-th torque current value, $i_{qs,j}^*$, with $\tilde{\theta} = 0$ based on the open-loop flux observer (21). Then, the HF voltage signal is injected with k-th tilted angle value, $\theta_{h,k}$. In this case, ϵ_{comp} can be computed by averaging ϵ over a period. Afterwards, we intentionally introduce a small positive perturbation $\tilde{\theta}_{int}$ in position as $\hat{\theta}_e = \theta_e + \tilde{\theta}_{int}$ to obtain ϵ^+ by averaging ϵ. Introduce a negative perturbation as $\hat{\theta} = \theta - \tilde{\theta}_{int}$ to obtain ϵ^-. At this point, we can compute the sensitivity as $k_e = \frac{\epsilon^+ - \epsilon^-}{2\tilde{\theta}_{int}}$. The entire process is looped for all k and then for all j. Finally, two 2D datasets of k_e v.s θ_h and ϵ_{comp} v.s θ_h are obtained for each $i_{qs,j}^*$. For each value of $i_{qs,j}$, the θ_h that yields the largest magnitude of k_e is chosen to construct the first LUT. With θ_h determined for all i_{qs}^*, the corresponding values of k_e and ϵ_{comp} can be found in the dataset to build the rest two LUTs.

The perturbed convergence analysis procedure above exploits the feasible operating range for a given i_{ds}^*. To further enlarge the operating range, we can increase the constant value i_{ds}^*, which is equivalent to increasing the saturation saliency level. However, there is a certain trade-off. When i_{ds}^* is getting larger, the motor operation becomes less efficient and the enlargement of feasible operating region becomes less significant. Overall, the problem 1 can be readily addressed using the entire process above.

The final HFSI speed observer that takes the error signal (19) as input and passes through PLL can be expressed as

$$\begin{aligned} \hat{\omega}_s &= (K_p + \frac{K_i}{s})\epsilon_{HFSI}, \\ \hat{\omega}_r &= \hat{\omega}_s - \frac{R_r i_{qs}}{L_r i^*_{ds}}, \end{aligned} \tag{22}$$

where the slip frequency is computed under the assumption of constant flux operation.

Algorithm 1: Perturbed Convergence Analysis

Input: i^*_{ds}, V_h, $i^*_{qs,all} = i_{qs,low} : \delta i : i_{qs,upp}$, $\theta_{h,all} = \theta_{h,low} : \delta\theta : \theta_{h,upp}$
Output: $f_1(i^*_{qs})$,$f_2(i^*_{qs})$,$f_3(i^*_{qs})$

for $i^*_{qs,j}$ in $i^*_{qs,all}$ **do**
  Implement current control with i^*_{ds} and $i^*_{qs,j}$ using $\hat{\theta}_e = \theta_e$ from open-loop flux observer (21),
  for $\theta_{h,k}$ in $\theta_{h,all}$ **do**
    Inject HF voltage signal (13) with tilted injection angle $\theta_{h,k}$,
    Record ϵ computed from (15) with $\tilde{\theta}_e = 0$ for several seconds and take the average to obtain $\epsilon_{comp}(i^*_{qs,j}, \theta_{h,k})$,
    Intentionally introduce a small positive perturbation $\tilde{\theta}_{int}$ in position estimation as $\hat{\theta}_e = \theta_e + \tilde{\theta}_{int}$,
    Record ϵ for several seconds and compute the average as ϵ^+,
    Introduce negative perturbation $-\tilde{\theta}_{int}$ in position estimation as $\hat{\theta}_e = \theta_e - \tilde{\theta}_{int}$.
    Record ϵ for several seconds and compute the average as ϵ^-
    Compute slope gain $k_e(i^*_{qs,j}, \theta_{h,k}) = \frac{\epsilon^+ - \epsilon^-}{2\tilde{\theta}_{int}}$
  end
end

B. Unified Observer

In order to achieve speed-sensorless control over the full speed range and solve for problem 2, we further propose the unified observer shown in Fig. 3, which combines the HFSI estimator operating at zero-to-low frequency range and the AFO operating at medium-to-high frequency range.

By comparing (22) and (9), we notice that the HFSI estimates the rotor flux speed while the AFO estimates the derivative of the rotor speed directly. Therefore, we propose various modifications to enable a smooth transition between two observers during operations. The final unified observer can be represented, in the $dq\hat{r}$ frame, as follows

$$\dot{\hat{\boldsymbol{x}}} = \mathbf{A}(\hat{\omega}_s)\hat{\boldsymbol{x}} + \mathbf{B}\boldsymbol{v}_{dqs} + \mathbf{L}(\boldsymbol{y} - \hat{\boldsymbol{y}}), \quad \hat{\boldsymbol{y}} = \mathbf{C}\hat{\boldsymbol{x}}, \tag{23a}$$

$$\dot{\hat{\omega}}_r = (K_p + \frac{K_i}{s})\epsilon^*, \quad \hat{\omega}_s = \hat{\omega}_r + \frac{L_m R_r}{L_r L_s \sigma}\frac{\hat{\lambda}_{\widehat{qs}}}{\hat{\lambda}_{\widehat{dr}}}, \tag{23b}$$

$$\epsilon^* = \begin{cases} i_{\widehat{qs}} - \hat{i}_{\widehat{qs}}, & \text{if } |\hat{\omega}_s| \geq \delta \\ C_{\text{lead}}(s)\epsilon_{\text{HFSI}}, & \text{otherwise} \end{cases} \tag{23c}$$

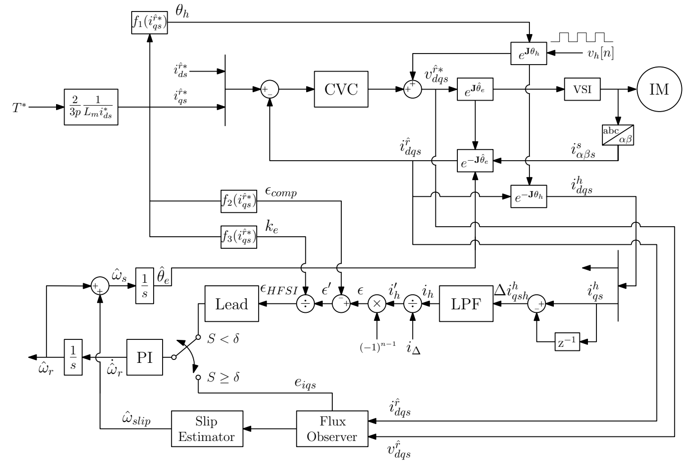

Fig. 3: Block diagram for unified observer.

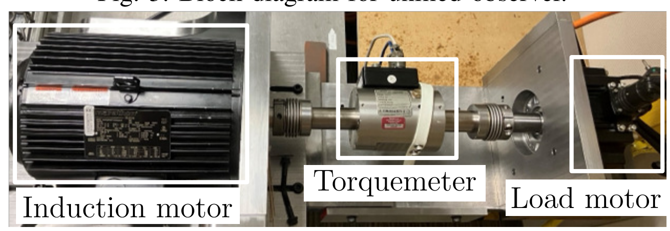

Fig. 4: Experimental testbed setup for IM.

TABLE I: Induction motor parameters

Parameter	Nominal Value
Stator resistance R_s	0.300 Ω
Rotor resistance R_r	0.263 Ω
Magnetizing inductance L_m	0.042 H
Stator inductance L_s	0.0434 H
Rotor inductance L_r	0.0442 H
Moment of inertia J	0.0285 kgm^2
Rated current I_b	20 A
Rated torque T_b	19 Nm
pole pairs p	2

where δ is a user-defined switching threshold and the magnitude of $|\hat{\omega}_s|$ indicates the observability [11]. The combined error signal ϵ^* is switched between HFSI and AFO according to $|\hat{\omega}_s|$ and then goes through a PI regulator to output the derivative of estimated speed. A lead compensator $C_{\text{lead}}(s) = \frac{\alpha_c \tau s + 1}{\tau s + 1}$ is added for HFSI error to make up the 90° phase delay brought by integrating $\dot{\hat{\omega}}_r$. Compared to switching on the speed estimate, switching on the estimated speed derivatives guarantees a smooth estimation during transition and the stability of the closed-loop system.

IV. Experiment

This section presents the experimental results on an IM testbed as shown in Fig. 4. It consists of a MyWay AC-DC-AC inverter and a Marathon three-phase IM that is coupled to an MR-J4 servomotor by torque sensor. The IM is operating in torque-controlled mode while the servomotor is in speed-controlled mode. The nominal values of the IM's parameters are shown in the Table. I. During experiments, a dSPACE SCALEXIO LabBox executes the data acquisition, real-time estimation, controller implementation, and PWM generation.

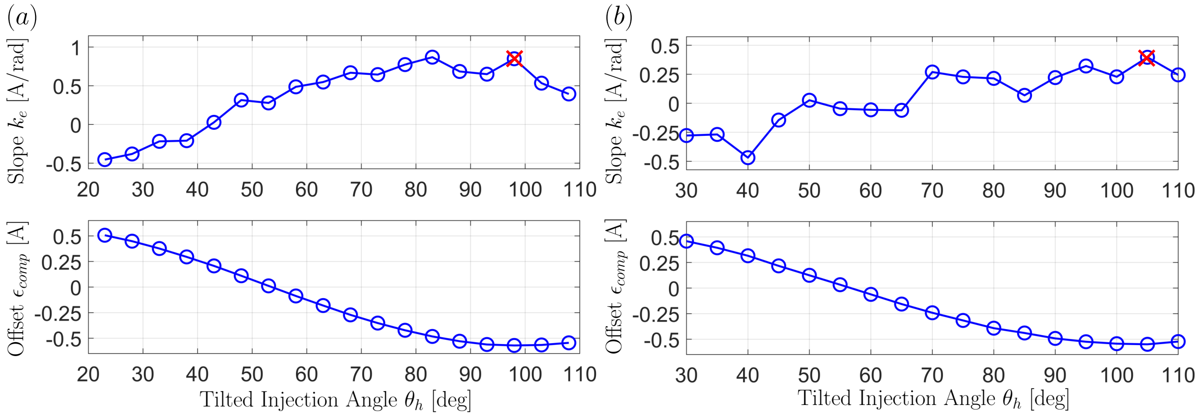

Fig. 5: (a) k_e and ϵ_{comp} v.s θ_h for $i_{ds}^* = 13\text{A}, i_{qs}^* = 5\text{A}$. (b) k_e and ϵ_{comp} v.s θ_h for $i_{ds}^* = 13\text{A}, i_{qs}^* = 6\text{A}$.

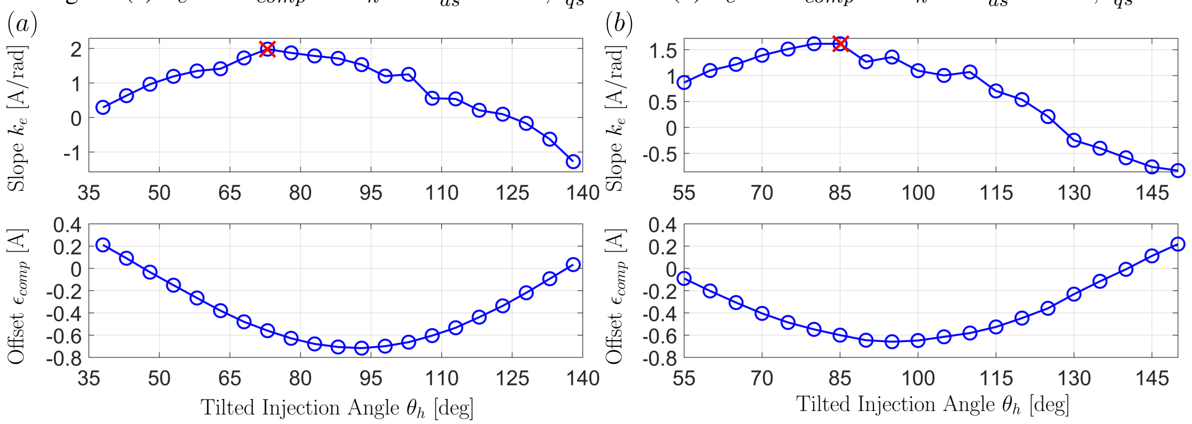

Fig. 6: (a) k_e and ϵ_{comp} v.s θ_h for $i_{ds}^* = 15\text{A}, i_{qs}^* = 5\text{A}$. (b) k_e and ϵ_{comp} v.s θ_h for $i_{ds}^* = 15\text{A}, i_{qs}^* = 6\text{A}$.

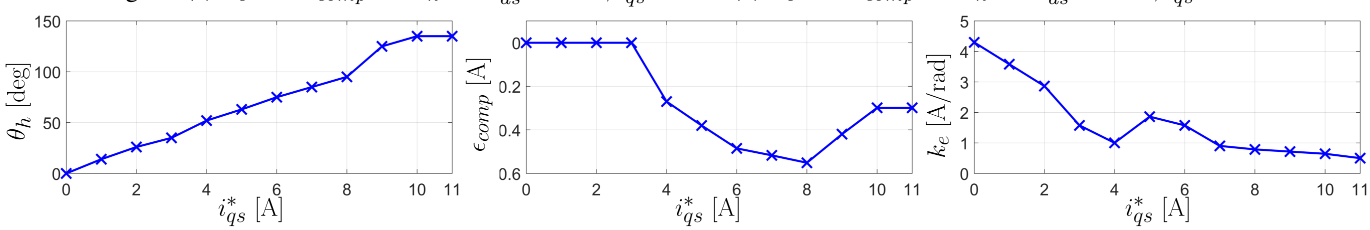

Fig. 7: Three LUTs for tilted injection angle θ_h, error compensation offset ϵ_{comp} and scaling gain k_e.

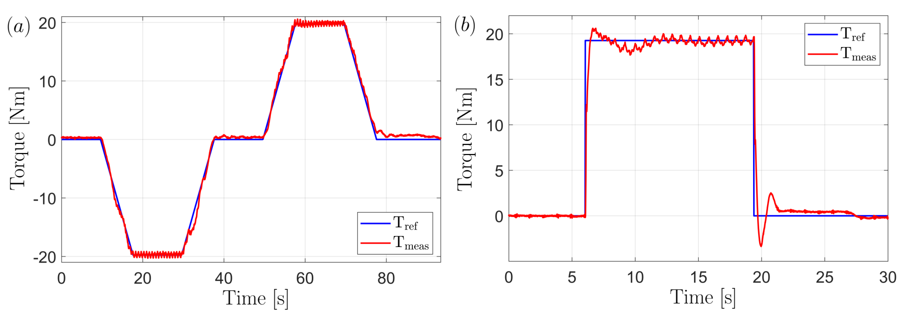

Fig. 8: (a) HFSI ramp torque test. (b) HFSI step torque test.

The sampling frequency and switching frequency are both 10 kHz.

A. Perturbed Convergence Analysis

The experimental perturbed convergence analysis in Algorithm. 1 is implemented to exploit the operating limit. The load machine is commanded at zero speed. Square-wave HF voltage injection magnitude is selected to be 50V and the frequency is 5kHz. The perturbation angle is set to $\tilde{\theta}_{int} = 2$ deg and the i_{qs}^* interval is 1 A. Fig. 5 and Fig. 6 illustrate the perturbed convergency analysis result for $i_{ds}^* = 13\text{A}, 15\text{A}$ and $i_{qs}^* = 5\text{A}, 6\text{A}$. First, we can see that both ϵ_{comp} are close to a smooth sinusoidal waveform with respect to θ_h as computed by (18), which validates the Taylor expansion form. The red-cross points are the tilted angles with maximum k_e magnitude

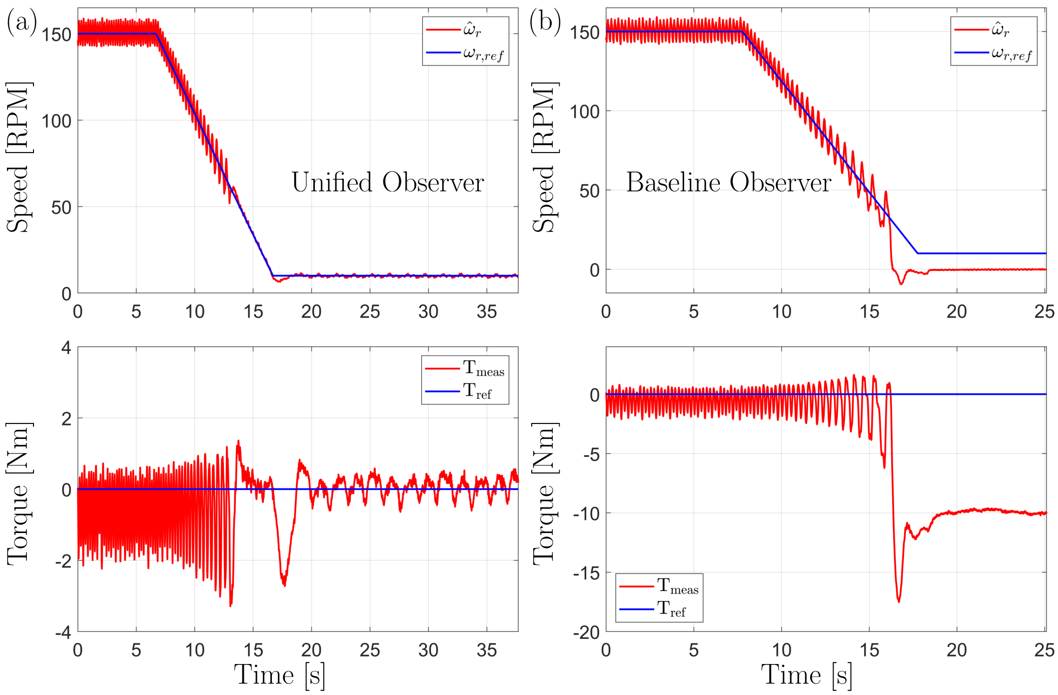

Fig. 9: Experimental results of test 1: from high speed to maintaining low frequency. (a) Speed and torque response of unified observer. (b) Speed and torque response of baseline AFO.

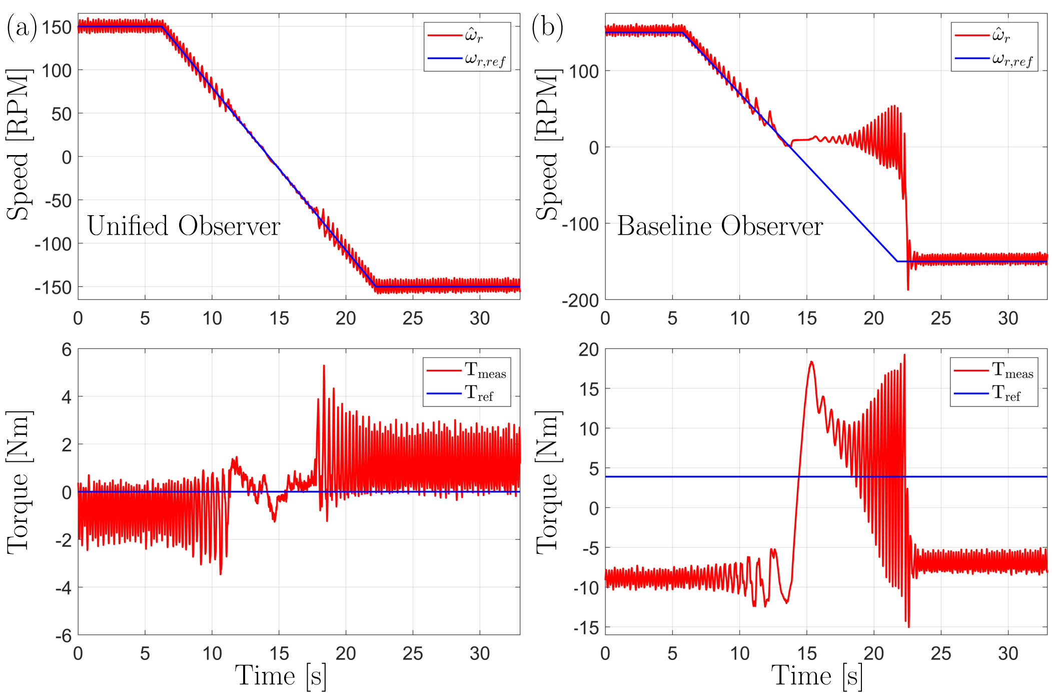

Fig. 10: Experimental results of test 2: from high speed to crossing zero frequency. (a) Speed and torque response of unified observer. (b) Speed and torque response of baseline AFO.

selected for the LUT. We can observe in Fig. 5 that optimal k_e decreases from 0.87 to 0.39 as i_{qs}^* increases from 5 A to 6 A and finally lead to infeasibility for i_{qs}^* larger than 6 A. Therefore, we can conclude that the feasible operating range for $i_{ds}^* = 13$ A is $-6 \sim 6$ A. By comparing Fig. 5 and Fig. 6, it can be seen that both optimal k_e value becomes significantly larger with larger i_{ds}^*, which enhances the feasibility as we expect. Accordingly, we select $i_{ds}^* = 15$ A as the constant flux reference to extend the operation range. The final 3 LUTs as (20) are shown in Fig. 7 where torque current limit is extended to $i_{qs}^* = 11\text{A}$, corresponding to the rated torque $19\ \text{Nm}$. For negative i_{qs}^*, we can simply negate the tilted injection angle θ_h and ϵ_{comp} when computing error signal due to symmetry.

Using the final three LUTs, we test the dynamic performance of closed-loop HFSI sensorless control as shown in Fig. 8. Fig. 8a shows a ramp torque test where the torque reference command gradually decreases from zero to negative rated torque value, $-19\ \text{Nm}$, gets back to zero, increases to positive rated value, $19\ \text{Nm}$, and then go back to zero under closed-loop sensorless control. It can be observed that the actual generated torque can accurately follow the reference with a satisfactory dynamic performance. Fig. 8b illustrates the performance of a step rated torque test where the actual generated torque can stably approach the desired torque with some transient. Both tests validate the proposed perturbed convergence analysis procedure and the usage of 3 LUTs for closed-loop HF voltage injection sensorless control.

B. Unified Observer

Fig. 3 shows the entire block diagram for the proposed unified observer where the HFSI error signal ϵ_{HFSI} is computed using the LUTs obtained in Sec. IV-A. The unified observer is implemented with switching threshold $\delta = 12.56\ \text{rad/s}$, which is determined from benchmarking against baseline AFO. The PI regulator in PLL and additional lead compensator are designed such that the estimation bandwidth is 2 Hz. Fig. 9 illustrates the results where the IM starts with $150\ \text{RPM}$ and gradually decrease to $10\ \text{RPM}$ with zero torque reference command. In Fig. 9b, the speed estimation of pure AFO diverges when the stator frequency is too small due to lack of observability. This helps us determine the switching threshold as $\delta = 2$ Hz beyond which the AFO part can perform a satisfactory estimation. In Fig. 9a, it can be observed that the unified observer can estimate the speed accurately over the entire profile and follow the torque command thanks to the proposed switching approach.

Fig. 10 shows another test where the IM starts with $150\ \text{RPM}$ and goes to $-150\ \text{RPM}$ driven by load machine with zero torque reference command. Similarly, the baseline AFO becomes unstable when the speed is approaching to zero. Meanwhile, the unified observer is capable of estimating the speed and regulating the torque through the two switches accurately and smoothly for whole speed range, which has demonstrated the effectiveness of our proposed switching algorithm. Note that there is a oscillating discrepancy of torque generation only in the AFO active region, which is mainly due to the model parameter mismatch in (23). However, this doesn't affect the dynamic performance during transition. The torque values can be more consistent if the parameters can be adapted to be more accurate.

V. Conclusion

This paper proposed a perturbed convergence analysis to extend the torque capability of HFSI sensorless IM control by optimizing tilted injection angle for maximum sensitivity of an error signal w.r.t. position estimation error. A novel unified observer is further proposed that combines the HFSI estimator and a baseline AFO for smooth control of IM at full speed range. Experiments validate the effectiveness of the proposed method.

References

[1] D. W. Novotny and T. A. Lipo, *Vector control and dynamics of AC drives*. Oxford university press, 1996, vol. 41.

[2] J. Holtz, "Sensorless control of induction motor drives," *Proceedings of the IEEE*, vol. 90, no. 8, pp. 1359–1394, 2002.

[3] F. Briz, M. W. Degner, A. Diez, and R. D. Lorenz, "Measuring, modeling, and decoupling of saturation-induced saliencies in carrier-signal injection-based sensorless ac drives," *IEEE Transactions on Industry Applications*, vol. 37, no. 5, pp. 1356–1364, 2001.

[4] J. Holtz, "Sensorless control of induction machines—with or without signal injection?" *IEEE transactions on industrial electronics*, vol. 53, no. 1, pp. 7–30, 2006.

[5] P. L. Jansen and R. D. Lorenz, "Transducerless field orientation concepts employing saturation-induced saliencies in induction machines," *IEEE Transactions on Industry Applications*, vol. 32, no. 6, pp. 1380–1393, 1996.

[6] Y.-D. Yoon and S.-K. Sul, "Sensorless control for induction machines based on square-wave voltage injection," *IEEE Trans. on Power Electronics*, vol. 29, no. 7, pp. 3637–3645, 2013.

[7] I. Hwang, Y.-C. Kwon, and S.-K. Sul, "Enhanced dynamic operation of heavily saturated ipmsm in signal-injection sensorless control with ancillary reference frame," *IEEE Transactions on Power Electronics*, vol. 38, no. 5, pp. 5726–5741, 2022.

[8] Y.-C. Kwon, J. Lee, and S.-K. Sul, "Extending operational limit of ipmsm in signal-injection sensorless control by manipulation of convergence point," *IEEE Transactions on Industry Applications*, vol. 55, no. 2, pp. 1574–1586, 2018.

[9] K. Ide, J.-I. H. J.-I. Ha, M. Sawamura, H. Iura, and Y. Yamamoto, "A novel hybrid speed estimator of flux observer for induction motor drives," in *Industrial Electronics, 2002. ISIE 2002. Proceedings of the 2002 IEEE International Symposium on*, vol. 3. IEEE, 2002, pp. 822–827.

[10] Z. Q. Zhu and X. M. Wu, *Sensorless Control of Permanent Magnet Synchronous Machine Drives*. John Wiley & Sons, 2023.

[11] P. Vaclavek, P. Blaha, and I. Herman, "Ac drive observability analysis," *IEEE Transactions on Industrial Electronics*, vol. 60, no. 8, pp. 3047–3059, 2012.